Matrix Element and Strong Electron Correlation Effects in ARPES from Cuprates

A. Bansil[1], R.S. Markiewicz[1], C. Kusko[1], M. Lindroos[1,2], and S. Sahrakorpi[1]
1. Physics Department, Northeastern University, Boston Massachusetts 02115, USA
2. Institute of Physics, Tampere University of Technology, 33101 Tampere, Finland

We discuss selected results from our recent work concerning the ARPES (angle-resolved photoemission) spectra from the cuprates. Our focus is on developing an understanding of the effects of the ARPES matrix element and those of strong electron correlations in analyzing photointensities. With simulations on $Bi_2Sr_2CaCu_2O_{8+\delta}$ (Bi2212), we show that the ARPES matrix element possesses remarkable selectivity properties, such that by tuning the photon energy and polarization, emission from the bonding or the antibonding states can be enhanced. Moreover, at low photon energies (below 25 eV), the Fermi surface (FS) emission is dominated by transitions from just the O-atoms in the CuO_2 planes. In connection with strong correlation effects, we consider the evolution with doping of the FS of $Nd_{2-x}Ce_xCuO_{4\pm\delta}$ (NCCO) in terms of the t-t'-U Hubbard model Hamiltonian. We thus delineate how the FS evolves on electron doping from the insulating state in NCCO. The Mott pseudogap is found to collapse around optimal doping suggesting the existence of an associated quantum critical point.

I. INTRODUCTION

Angle resolved photoemission spectroscopy (ARPES) has proven to be a powerful technique for probing the properties of the superconducting cuprates. In analyzing the data, it is important to keep in mind the effects of the ARPES matrix element as well as those of the strong electron correlations[1,2,3,4,5,6,7,8,9,10]. With this motivation, we present in this article some of our recent work directed at understanding these effects in the cuprates.

In connection with matrix element effects, we discuss the ARPES intensity from initial states in the vicinity of the $M(\pi,0)$ symmetry point in tetragonal Bi2212. For this purpose, one-step photointensity calculations for several different initial state energies for both the bonding and the antibonding bands over the photon energy range of 10-100 eV are presented. These results give insight into how the cross-sections for exciting these bands vary with the photon energy on the one hand, and the character and energy of the initial state on the other hand. We comment on systematics in the theoretical spectra, and provide examples of specific energies or energy ranges, which are well-suited for highlighting various interesting spectral features. We also consider the extent to which different sites in the unit cell contribute to the photointensity. This question is addressed via computations of the dipole matrix element for exciting the bonding or the antibonding portion of the Fermi surface of Bi2212 throughout the Brillouin zone for two different polarizations of the incident light. Here the results show a remarkable selectivity of the spectra with respect to the O-sites for low photon energies. On the whole, our computations indicate that by fine tuning photon energy and/or polarization, ARPES can help zoom in on specific states and/or sites in the cuprates. We note that the methodology used here has been described in detail in our earlier publications on the cuprates[1,2,3,4,5,6,11,12]. The crystal potential used in Bi2212 is the same as that used in Ref. 2 and, consistent with ARPES data, it does not contain Bi-O pockets around the M-point.

Turning to the electron doped cuprates, we discuss the properties of the t-t'-U Hubbard model Hamiltonian, keeping in mind the recent doping dependent ARPES data on NCCO. The analysis is carried out using the framework of the mean-field Hartree-Fock (HF) as well as that of the self-consistent renormalization (SCR) theory to include the effect of fluctuations. The relevant details of methodology are given in Refs. 8, 9, and 13. It should be noted that our comparisons between theory and experiment on NCCO do not include the effects of the ARPES matrix element, but are considered to be adequate for our purposes of gaining a handle on the overall topology of the FS. An effort to include the ARPES matrix element in the presence of strong correlations is in progress and will be taken up elsewhere. The experimental band dispersions are used to fit the doping dependence of U, which is found to be quite similar for the HF and the SCR computations. In this way, we determine the evolution of the FS and the Mott pseudogap in NCCO. This study also gives insight into the stability of the uniformly doped phase (with respect to the formation of competing nano-scale orders) upon electron vs. hole doping.

II. SELECTIVITY PROPERTIES OF THE ARPES MATRIX ELEMENT IN BI2212

Figure 1 presents one-step ARPES photointensities for tetragonal Bi2212 in the vicinity of the $M(\pi,0)$-symmetry point at four illustrative initial state energies. The $\mathbf{k}_\parallel$-values are chosen for each energy so that the antibonding (A) or the bonding (B) band is excited as indicated by open circles in the insert. At energies E_1 and E_2, the A-band is electron-like around Γ, while at E_4, it is hole-like around $X(\pi,\pi)$. Referring to energies, E_2 through E_4, the six topmost curves in the figure show that the ARPES intensity from either the A or the B band is more or less similar for small (compared to the bilayer splitting) changes in energy. However, the intensity is seen to vary dramatically with photon energy

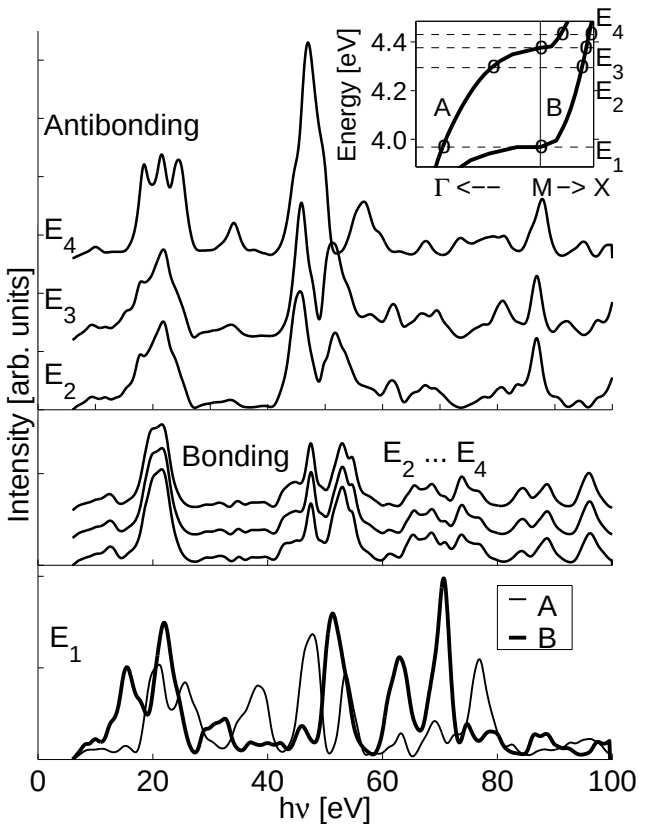

FIG. 1: Theoretical one-step ARPES photointensities for emission from the antibonding (A) and bonding (B) bands in the vicinity of the $M(\pi,0)$-point as a function of the photon energy $h\nu$ in Bi2212. Insert shows the A and B bands and four initial state energies E_1-E_4 at which results for intensities are shown (open circles mark the relevant $\mathbf{k}_\parallel$-values). Incident light is assumed to be polarized along the x-axis, defined as the direction of the Cu-O bonds.

and these variations extend up to the 100 eV upper energy limit considered. For example, the A-band is quite intense in energy ranges around 20 eV, 47 eV and 88 eV. The relative intensities of the A and B bands are seen to differ greatly. For example, A is far more intense than B at around 47 eV and 88 eV, while the case is opposite around 95 eV. Such special photon energies can help focus on the properties of the A or the B band in the ARPES spectra. The theoretically predicted enhancement of the A to B features at 47 eV has been exploited recently by Chuang et al.[6] to resolve bilayer splitting throughout the doping range from overdoped to underdoped samples, and to adduce that some coherence of electronic states between the CuO_2 planes persists in Bi2212 even in the underdoped regime.

The preceding discussion makes it clear that the ARPES cross-sections for excitation of states near the Fermi energy (E_F) depend strongly on photon energy and that these photon energy dependencies differ substantially between the A and B type states. It is interesting as well to consider how these cross-sections vary with the initial state energy. A sensible energy scale in this connection is that provided by the bilayer splitting, $\Delta_{\rm bilayer}$. The superconducting energy scale, $\Delta_{\rm super}$, is $\approx$ 30-50% of $\Delta_{\rm bilayer}$. For this purpose, we compare results in Figure 1 at the energy E_1 (lowest panel) with those at $E_2 - E_4$ (upper panels), where E_1 is separated from $E_2 - E_4$ by about $\Delta_{\rm bilayer}$. We see, for example, that in going from E_4 to E_1, the A-band develops peaks at around 38 and 77 eV, while the B-band displays new peaks at around 18, 63 and 70 eV. On the other hand, some energy ranges are less sensitive to changes in the initial state energy, e.g. the region from 60-75 eV for the A-band and the regions from 35-45 eV and above 75 eV for the B-band. These considerations will be important in identifying energy regions, which may be particularly suitable for implementing recent proposals[14] for developing ARPES as a self-energy spectroscopy, where the role of $\mathbf{k}_\parallel$ and energy dependencies of the ARPES matrix element needs to be minimized.

The ARPES matrix element also exhibits remarkable site-selectivity properties in Bi2212 in that, for low photon energies ($h\nu \leq$ 25 eV), the intensity for emission around E_F is dominated by excitations from just the O-sites in the CuO_2 planes, even though the relevant initial states possess an admixture of Cu and O character. Our analysis suggests that at higher photon energies, the contribution to intensity from Cu sites increases, and at around 40 eV, the Cu and O contributions are roughly comparable.[5] As discussed elsewhere[2,5,15], insight in this regard can be obtained by considering the square of the dipole matrix element, i.e.

$$|M|^2 \equiv |<\Psi_f|\mathbf{A}\cdot\mathbf{p}|\Psi_i>|^2 \qquad (1)$$

where $\mathbf{A}$ is the vector potential of the incident photon field, $\mathbf{p}$ is the momentum operator, and Ψ_i and Ψ_f are the bulk crystal wavefunctions of the initial and final states involved. Fig. 2 presents the intensity based on Eq. 1 for emission from the antibonding as well as the bonding portions of the FS for two different polarizations of light. The contributions to the total intensity arising from the O-sites (denoted by O_{Cu}/thin solid line) and the Cu sites (thin dashed line) in the CuO_2 bilayers are shown. The contributions from other sites (not shown) are not always negligible as seen by comparing the total intensity curves (thick solid lines) with the sum of the thin curves, a point to which we return below. Incidentally, O contribution in Figs. 2(a) and 2(c) is slightly higher than the total intensity curve – this reflects interference effects between the contributions from different sites when the absolute value of the matrix element is taken in Eq. 1.

In looking at the results of Fig. 2, it is important to bear in mind the effect of symmetry on the dipole matrix element. In view of the direction of the polarization vector, the left hand side panels pick up only the part $M_y \equiv <\Psi_f|p_y|\Psi_i>$ of the momentum operator, $\mathbf{p}$, while the right hand side panels similarly yield $M_x \equiv <\Psi_f|p_x|\Psi_i>$. Comparing the total intensities in

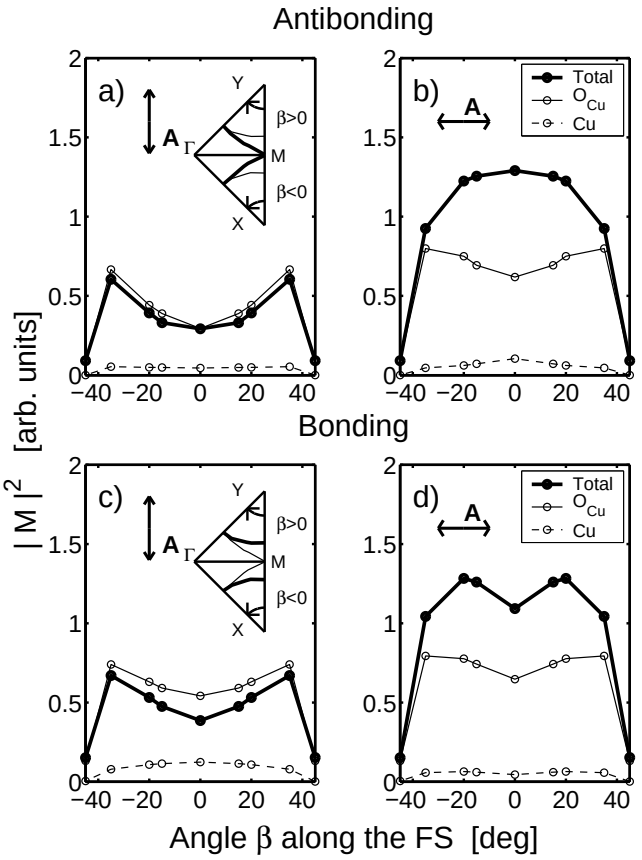

FIG. 2: ARPES intensity defined as the square of the dipole matrix element, $|M|^2$ (see Eq. 1), for excitation of initial states lying along the FS of Bi2212. Thick solid lines give total intensity, thin solid lines give partial contribution from just the O_{Cu} sites in the CuO_2 bilayers; the corresponding partial contribution from Cu sites is shown dashed. Photon energy is 22 eV. The right hand panels refer to light polarized along the Cu-O bond in x-direction (denoted by the double arrow of the vector potential $\mathbf{A}$), while in the left hand panels the polarization vector is rotated by 90^o. (a) and (b) consider excitation of states on the antibonding FS [thick solid line in the insert to (a)]. The $\mathbf{k}_\parallel$ values along the FS are defined by the angle β (inserts in a,c), where $\beta = 0^o$ corresponds to the $X(Y) - M$-direction, and $\beta = \pm 45^o$ corresponds to the $Y(X) - \Gamma$ direction. (c) and (d) similarly refer to the bonding FS. All intensities are normalized correctly relative to one another.

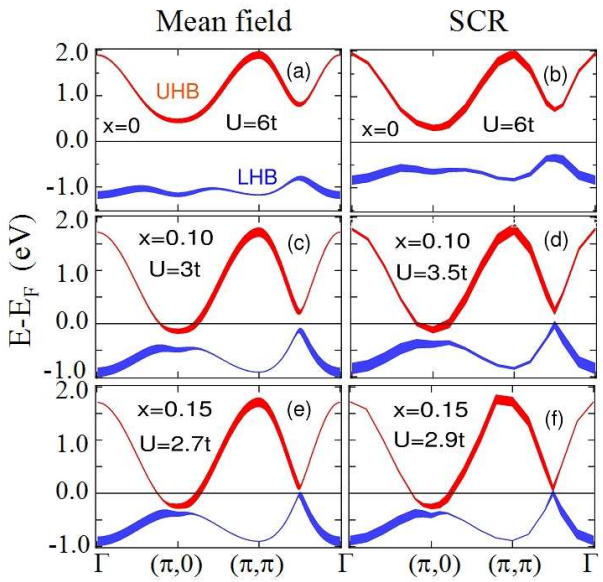

FIG. 3: Dispersion curves for NCCO within the t-t'-U Hubbard model, showing the evolution of the upper and lower Hubbard bands (denoted by UHB and LHB) with doping x. Results for the mean field computations are given in the left column, and for the mode coupling, self-consistent renormalization (SCR) theory in the right column. Values of x and U are marked in each panel. Thickness of bands denotes their spectral weight. Horizontal lines mark the Fermi energy.

(a) with (c), or in (b) with (d), we see thus that the squared absolute value of M_y is smaller than that of M_x for the antibonding as well as the bonding FS in the vicinity of the $M(\pi, 0)$-point. It is straightforward to show that the symmetry of the curves in Fig. 2 around $\beta = 0$ is tied to the mirror symmetry of the underlying tetragonal lattice through the $\Gamma - M$ line. The mirror symmetry through the $\Gamma - Y$ and $\Gamma - X$ lines, on the other hand, can be used to deduce that at $\beta = \pm 45^o$, $|M_x| = |M_y|$, so that the intensity at $\beta = \pm 45^o$ is the same for either horizontal or vertical polarization, as is seen to be the case with reference to various panels of Fig. 2.

Fig. 2 shows that the Cu contribution to the total intensity is quite small at ~ 22 eV photon energy for either polarization for both the bonding and the antibonding FS states throughout the Brillouin zone. The O_{Cu} contribution is seen to be substantial in all four cases. This is particularly the case for polarization along the y-direction in panels (a) and (c), suggesting that in the vicinity of the $M(\pi, 0)$-point the A_y polarized light would be well-suited for probing the character of O_{Cu} electrons. The results for the A_x-polarized light, in the right hand side panels (b) and (d) show a somewhat more complicated behavior in that significant contribution from other atoms (than O_{Cu}) in the unit cell is involved. Our analysis indicates that these additional contributions arise from O atoms in the Bi-O and Sr-O layers in the structure. Despite some uncertainty with respect to the extent to which Bi contributes to emission from the E_F in Bi2212, it seems then that A_x polarization will likely be more sensitive for investigating the properties of apical O-sites in the Sr-O planes.

III. MOTT GAP COLLAPSE IN NCCO

We now discuss briefly the issue of evolution of the electronic structure and FS of NCCO with doping and the related collapse of the Mott gap around optimal doping with reference to Figs. 3 and 4. As already noted, these results are based on the t-t'-U Hubbard model Hamiltonian, where the value of U has been used as a fitting parameter to reproduce the experimentally observed doping dependence of the FS in NCCO observed via ARPES experiments.

The mean field[8] and the SCR[9] results of Fig. 3 are seen to be quite similar, although the specific values of U needed in the two cases are somewhat different. The SCR computations are of course more satisfactory since the effects of fluctuations are incorporated. The mean field theory suffers from the well-known problem that it predicts the Neel temperature to be too high. However, when fluctuations are included (in the mode coupling approach), true long-range order only appears at $T = 0$, consistent with the Mermin-Wagner theorem, while a *pseudogap* opens up close to the mean-field Neel transition due to short-range antiferromagnetic order. The undoped system ($x = 0$) displays a wide gap between the UHB and the LHB. At intermediate doping ($x = 0.10$), the band gap is substantially reduced and electron pockets appear around the $(\pi, 0)$-point in the UHB. At optimal doping ($x = 0.15$), the band gap has essentially disappeared, and recalling that thin lines possess little spectral weight in Fig. 3, the band dispersions resemble those for the uncorrelated case with a large hole FS sheet centered around the (π, π)-point. It is important to observe that our analysis indicates that the Hubbard U must *decrease* significantly with doping – by about a factor of two from the value of $6t$ in the undoped case to around $3t$ in the optimally doped system[16]. Interestingly, our finding that the Mott pseudogap collapses around optimal doping, where the staggered magnetization goes to zero and the $T = 0$ Neel ordered state terminates, suggests the presence of an associated quantum critical point (QCP) in the spectrum. The manifestation of optimal superconductivity in the vicinity of this QCP is consistent with results in other magnetic materials[17], including hole-doped cuprates[18].

Insight into the preceding discussion is provided by the illustrative example of Figure 4, which compares computed FS maps for the mean field (top right) and SCR (bottom left) calculations, with the corresponding experimental[19] ARPES intensities (top left) at intermediate doping $x = 0.10$. In the mean-field calculations, a small second-neighbor hopping t'' has been included to better fit the shape of the FS near the nodal point, and the data are broadened to reflect experimental resolution. We emphasize that the effects of the ARPES matrix element, discussed in the preceding section, are not included in these computations. Nevertheless, we expect accord between theory and experiment at the level of providing the correct topology of the FS. This indeed is seen to be the case. Recalling Fig. 3, both theory and experiment display the electron pocket around $(\pi, 0)$ [with a symmetrically placed pocket located at $(0, \pi)$], arising from the doping of the UHB. Additionally, as the Mott pseudogap decreases, a second *hole*-like Fermi surface appears near $(\pi/2, \pi/2)$ coming from the LHB. Notably, evidence for two-band conduction has been found in this doping range.[20]

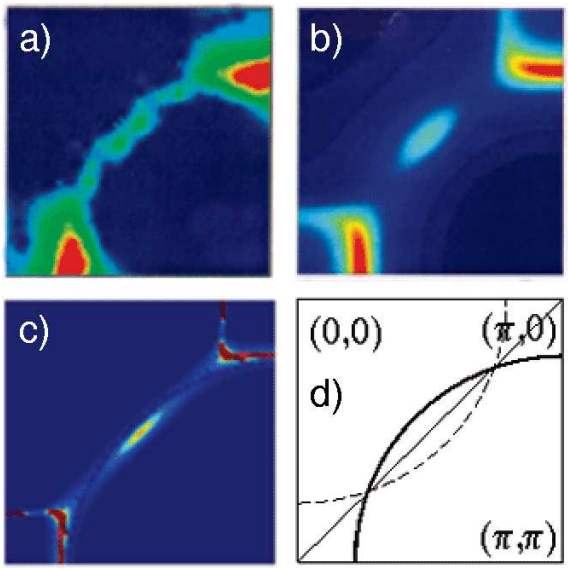

FIG. 4: Fermi surface of NCCO at $x = 0.10$. Experimental ARPES results for emission from the Fermi energy in (a) are compared with mean field (b), and SCR (c) computations. Frame (d) shows a schematic uncorrelated FS (thick solid line) and the related "shadow" FS (dashed line) obtained by folding the solid line around the magnetic zone boundary.

IV. SUMMARY AND CONCLUSIONS

In this article, we have briefly discussed two aspects of our recent work aimed at understanding the high-T_c cuprates via ARPES experiments: (i) Matrix element effects in ARPES spectra of Bi2212, and (ii) Evolution of electronic structure and FS of NCCO with electron doping.

In considering matrix element effects, we discuss two distinct types of selectivity properties of the ARPES matrix element. Firstly, depending on the character of the initial state involved, the ARPES matrix element can yield widely differing cross-sections as a function of the energy and polarization of the incident photons. This effect can be used to discriminate, for example, between the bonding and antibonding pieces of the FS in Bi2212. Such a theoretically predicted enhancement of antibonding to bonding intensity at 47 eV has in fact been exploited in Ref. 6 to adduce that the bilayer splitting in Bi2212 is surprisingly insensitive to doping and that some

coherence of electronic states persists across the CuO_2 bilayers even in the underdoped regime. Secondly, we show that the ARPES matrix element possesses remarkable "site-selectivity" in that the emission in the low photon energy range (5-25 eV) in Bi2212 is dominated by excitations from just the O-sites in CuO_2 planes throughout the (k_x, k_y)-plane. The polarization vector of the incident light may provide some sensitivity to O-sites in Bi-O and Sr-O planes. At higher photon energies (above 25 eV), Cu sites begin to progressively contribute to the ARPES intensity. These results suggest that ARPES could potentially allow one to focus on the properties of specific groups of electrons associated with various sites in the unit cell.

With regard to the electron doped cuprates, we have analyzed the evolution of the electronic structure and the FS of NCCO with doping within the framework of the t-t'-U Hubbard model Hamiltonian in the light of related ARPES experiments. Computations have been carried out both within the mean field Hartree Fock as well as the self-consistent renormalization frameworks. We show how the FS develops when electrons are added in the undoped insulating state: At first the electrons enter the upper Hubbard band around the $(0, \pi)$ and $(\pi, 0)$ points, but on further doping electrons also enter the lower Hubbard band first around the $(\pi/2, \pi/2)$ point. Finally, around optimal doping, the FS essentially resembles that of the uncorrelated state with a large (π, π) centered hole sheet. Notably, we find that the effective Hubbard U must decrease substantially with doping, such that the Mott pseudogap collapses around optimal doping, suggesting the existence of an associated quantum critical point in the spectrum. Our study also indicates that a uniformly doped antiferromagnetic state in the cuprates is likely more easily accessible via electron doping rather than through hole-doping, since in the latter case the system is unstable towards various competing orders (nano-scale phase separations).

Acknowledgments

This work is supported by the US Department of Energy contract DE-AC03-76SF00098, and benefited from the allocation of supercomputer time at NERSC, Northeastern University's Advanced Scientific Computation Center (ASCC), and the Institute of Advanced Computing (IAC), Tampere. One of us (S.S.) acknowledges Suomen Akatemia and Vilho, Yrjö ja Kalle Väisälän Rahasto for financial support.

[1] A. Bansil and M. Lindroos, Phys. Rev. Lett. **83**, 5154 (1999).
[2] M. Lindroos, S. Sahrakorpi and A. Bansil, Phys. Rev. B **65**, 054514 (2002).
[3] A. Bansil, M. Lindroos, S. Sahrakorpi, R. S. Markiewicz, G. D. Gu, J. Avila, L. Roca, A. Tejeda and M. C. Asensio, J. Phys. Chem. Solids 63, 2175 (2002).
[4] M. C. Asensio, J. Avila, L. Roca, A. Tejeda, G.D. Gu, M. Lindroos, R. S. Markiewicz and A. Bansil, Phys. Rev. B **67**, 014519 (2003).
[5] S. Sahrakorpi, M. Lindroos, and A. Bansil, Phys. Rev. B **68**, 054522 (2003).
[6] Y.-D. Chuang, A. D. Gromko, A.V. Fedorov,Y. Aiura, K. Oka, Y. Ando, M. Lindroos, R. S. Markiewicz, A. Bansil and D. S. Dessau, Submitted to Phys. Rev. B (2003).
[7] A. A. Kordyuk, S. V. Borisenko, T. K. Kim, K. A. Nenkov, M. Knupfer, J. Fink, M. S. Golden, H. Berger, and R. Follath, Phys. Rev. Lett. **89**, 077003 (2002).
[8] C. Kusko, R. S. Markiewicz, M. Lindroos, and A. Bansil, Phys. Rev. B**66**, 140513 (2002).
[9] R.S. Markiewicz, cond-mat/0308361 and cond-mat/0308469.
[10] A. Damascelli, Z.-X. Shen, and Z. Hussain, Rev. Mod. Phys. 75, 473 (2003).
[11] A. Bansil and M. Lindroos, J. Phys. Chem. Solids **56**, 1855(1995).
[12] M. Lindroos and A. Bansil, Phys. Rev. Lett. **75**, 1182(1995).
[13] T. Moriya, "Spin Fluctuations in Electron Magnetism", (Springer, Berlin, 1985).
[14] I. Vekhter and C. M. Varma, Phys. Rev. Lett. 90, 237003 (2003).
[15] S. Sahrakorpi, M. Lindroos and A. Bansil, Phys. Rev. B **66**, 235107 (2002).
[16] J. Kanamori, Prog. Theor. Phys. **30**, 275 (1963).
[17] N. D. Mathur, F. M. Grosche, S. R. Julian, I. R. Walker, D. M. Freye, R. K. W. Haselwimmer, and G. G. Lonzarich, Nature **394**, 39 (1998).
[18] J. L. Tallon, J. W. Loram, G. V. M. Williams, J. R. Cooper, I. R. Fisher, J. D. Johnson, M. P. Staines, and C. Bernhard, Phys. Stat. Sol. b**215**, 531 (1999).
[19] N. P. Armitage, F. Ronning, D. H. Lu, C. Kim, A. Damascelli, K. M. Shen, D. L. Feng, H. Eisaki, Z.-X. Shen, P. K. Mang, N. Kaneko, M. Greven, Y. Onose, Y. Taguchi, and Y. Tokura, Phys. Rev. Lett. 88, 257001 (2002).
[20] W. Jiang, S. N. Mao, X. X. Xi, X. Jiang, J. L. Peng, T. Venkatesan, C. J. Lobb, and R. L. Greene, Phys. Rev. Lett. 73, 1291 (1994).